Atmos. Chem. Phys. Discuss., 15, 12353–12387, 2015
www.atmos-chem-phys-discuss.net/15/12353/2015/
doi:10.5194/acpd-15-12353-2015

Atmospheric Chemistry and Physics
Open Access
Discussions

A solar signal in lower stratospheric water vapour?

T. Schieferdecker, S. Lossow, G. P. Stiller, and T. von Clarmann

Karlsruhe Institute of Technology, Institute for Meteorology and Climate Research, Karlsruhe, Germany

Received: 13 March 2015 – Accepted: 3 April 2015 – Published: 24 April 2015

Correspondence to: T. von Clarmann (thomas.clarmann@kit.edu)

Published by Copernicus Publications on behalf of the European Geosciences Union.

Abstract

A merged time series of stratospheric water vapour built from HALOE and MIPAS data between 60° S and 60° N and 15 to 30 km and covering the years 1992 to 2012 was analyzed by multivariate linear regression including an 11 year solar cycle proxy. Lower stratospheric water vapour was found to reveal a phase-shifted anti-correlation with the solar cycle, with lowest water vapour after solar maximum. The phase shift is composed of an inherent constant time lag of about 2 years and a second component following the stratospheric age of air. The amplitudes of the water vapour response are largest close to the tropical tropopause (up to 0.35 ppmv) and decrease with altitude and latitude. Including the solar cycle proxy in the regression results in linear trends of water vapour being negative over the full altitude/latitude range, while without the solar proxy positive water wapour trends in the lowermost stratosphere were found. We conclude from these results that a solar signal generated at the tropical tropopause is imprinted on the stratospheric water vapour abundances and transported to higher altitudes and latitudes via the Brewer–Dobson circulation. Hence it is concluded that the tropical tropopause temperature at the final dehydration point of air is also governed to some degree by the solar cycle. The negative water vapour trends obtained when considering the solar cycle impact on water vapour abundances can solve the water vapour conundrum of increasing stratospheric water vapour abundances at constant or even decreasing tropopause temperatures.

1 Introduction

Water vapour is one of the Earth's most important greenhouse gases, having the strongest longwave radiative forcing effect on the atmosphere (Kiehl and Trenberth, 1997). An increase of water vapour in the lower stratosphere leads to a warmer troposphere, further affecting global surface temperatures (Manabe and Strickler, 1964; Solomon et al., 2010). Mainly water vapour concentrations near the tropopause, particularly in the tropics, strongly influence surface climate (Riese et al., 2012), and increasing stratospheric concentrations intensify ozone loss in this atmospheric region (Stenke and Grewe, 2005). For these reasons it is of major importance to understand its trends and fluctuations on a global scale. It is generally accepted that the tropical tropopause temperature is the main driver of the amount of water vapour transported from the troposphere into the stratosphere (Fueglistaler et al., 2009). However, admittedly, the analysis of stratospheric and upper tropospheric water vapour trends is challenging given the fact that only few decades of global data are available. Particular issues of the ongoing discussion are the apparent inconsistencies between the time series measured above Boulder with frost point hygrometers (Hurst et al., 2011) and global satellite data (Hegglin et al., 2014); the sudden decrease in lower stratospheric water vapour mixing ratios observed in 2000/01 (Rosenlof and Reid, 2008; Randel et al., 2006) and in 2011/12 (Urban et al., 2014) as well as missing processes that constrain stratospheric water vapour (besides TTL temperature conditions and transport) (Rosenlof et al., 2001; Fueglistaler et al., 2013); a potential steep increase around 1990 that puts into question if a decoupling of stratospheric water vapour and tropical tropopause temperature trends on short timescales is possible (Fueglistaler, 2012); the role of deep and overshooting convection for the moistening of the stratosphere (Corti et al., 2008; Schiller et al., 2009); and finally the role of the Western Tropical Pacific cold trap for the transport of water vapour into the stratosphere (Holton and Gettelmann, 2001; Fueglistaler et al., 2005).

In this work, stratospheric H_2O records from the Halogen Occultation Instrument (HALOE) (Russell III et al., 1993) and the Michelson Interferometer for Passive Atmospheric Sounding (MIPAS, Fischer et al., 2008) have been used to analyze the lower stratospheric H_2O time series since 1992. The main characteristics of these two instruments are summarized in Sect. 2. These data sets have been harmonized in order to get a homogeneous H_2O record (Sect. 3). This merged long-term record has then been analyzed by means of multi-linear regression analysis (Sect. 4) in order to identify the processes controlling the variability of stratospheric water vapour. In Sect. 5 the results are critically discussed and put in context of results from other research groups. Section 6 aims at estimating the implications of our results for future research.

2 The empirical basis

While a large number of altitude-resolved H_2O records inferred from limb emission or occultation measurements (e.g. Hegglin et al., 2013), as well as merged data sets (e.g. Froidevaux et al., 2015) exist, for this study stratospheric H_2O records from HALOE (Russell III et al., 1993) and MIPAS (Fischer et al., 2008) have been used. The reason is that both these instruments provided H_2O measurements at near-global coverage and that their mission periods were nicely complementary, with a sufficiently long overlap period for data harmonization. Inclusion of further instruments would have implied an additional risk of artefacts due to unknown differences in data characteristics.

2.1 HALOE

The Halogen Occultation Instrument (HALOE) (Russell III et al., 1993) is a solar occultation infrared radiometer for measurement of composition and temperature of the middle atmosphere. It recorded atmospherically attenuated solar radiance in four channels between 996 and 4081 cm^{-1}. HALOE was a payload of the Upper Atmosphere Research Satellite (UARS) and was operational from 11 October 1991 to 21 November 2005. With about 15 UARS orbits per day and one sunrise and one sunset measurement per orbit, up to about 10 800 vertical profiles of each target quantity could be measured per year. One of the target species measured by HALOE is H_2O, for which an altitude resolution of 2 to 3 km is reported (Russell III, 1995; Hegglin et al., 2013). In this work we use HALOE data Version 19, which was discussed in Kley et al. (2000) and Hegglin et al. (2013), where a small dry bias is reported for the altitude range relevant to this paper. Problems with HALOE water vapour retrievals of an earlier data version due to aerosol have been reported by Hervig et al. (1995) but problematic cases discussed there were no longer present in the data set we used and thus seem to have been removed (Steele and Turco, 1997). During its 14 year lifetime, HALOE H_2O measurements were frequently validated (Harries et al., 1996; Dessler and Kim, 1999).

2.2 MIPAS

The Michelson Interferometer for Passive Atmospheric Sounding (MIPAS, Fischer et al., 2008) is a limb emission mid-infrared Fourier Transform spectrometer designed for limb-sounding of the composition and temperature of the middle atmosphere. Its spectral coverage is 685 to 2410 cm^{-1}. MIPAS was a core instrument of the Envisat research satellite which was launched into a polar sun-synchronous orbit on 1 March 2002. The MIPAS data record covers the time from July 2002 to April 2012, with a data gap in 2004. In the first part of the mission (2002–2004) MIPAS recorded high-resolution (HR) spectra (apodized resolution 0.05 cm^{-1}). In March 2004 operation was interrupted due to problems with the interferometer slide until in January 2005 operation was resumed, however at reduced spectral resolution (RR, 0.121 cm^{-1} after apodization). In turn, the shorter optical path difference associated with the reduced spectral resolution measurements allowed for a denser tangent altitude grid and along with this a better vertical resolution, which is 4.0 km in the middle stratosphere as opposed to 4.5 km for the high spectral resolution measurements. With 14.4 orbits per day and 74 (96) limb scans per orbit in HR (RR) mode, MIPAS recorded 1065 (1382) profiles per day.

The MIPAS H_2O data used here were produced with a dedicated research processor developed and operated by the Institute of Meteorology and Climate Research (IMK) team in Karlsruhe, Germany, in cooperation with the Instituto de Astrofísica de Andalucía-CSIC in Granada, Spain (von Clarmann et al., 2003). The MIPAS H_2O retrieval and validation is reported in Milz et al. (2005, 2009); von Clarmann et al. (2009); Stiller et al. (2012a). In this paper we have used data versions V5h_H2O_20 for the HR measurements and V5r_H2O_220/221 for the RR measurements. Versions 220 and 221 are scientifically equivalent but carry different version numbers to maintain traceability of data processing details.

3 The harmonized H_2O record

The combined HALOE-MIPAS H_2O record covers more than two decades. Both the HALOE and the MIPAS data sets have been filtered according to provider-defined criteria: trip angle and lockdown angle issues for HALOE; and low averaging kernel diagonal values and visibility flag for MIPAS. Further, in order to avoid artefacts, homogenization of the data is important. The following issues have been tackled: (1) artefacts due to Pinatubo aerosol, (2) different altitude resolution and (3) biases and stability.

3.1 Pinatubo

The eruption of Mount Pinatubo on 15 June 1991 brought enormous amounts of aerosol into the stratosphere. This aerosol layer affected the radiative transfer of solar radiation through the atmosphere and led to artefacts in the HALOE analysis (Steele and Turco, 1997). Thus, HALOE data from the first five months have been discarded and data since March 1992 have been used.

3.2 Altitude resolution

For harmonization with respect to altitude resolution we use the method suggested by Connor et al. (1994) and described in detail for application to MIPAS profiles by Stiller et al. (2012a). The better resolved HALOE profile is degraded with a representative MIPAS averaging kernel (see Rodgers, 2000, for a detailed discussion of the concept of averaging kernels) to provide a HALOE H_2O profile as MIPAS with its inferior altitude resolution would have seen it. Representative MIPAS averaging kernels were constructed for each latitude band of ten degrees coverage and for each season (Fig. 1). Details of the construction of representative averaging kernels are reported in Schieferdecker (2015). Along with this degradation, HALOE data were resampled on the MIPAS altitude grid which has a one kilometer gridwidth in the altitude range relevant to this study.

Figure 2 shows the combined time series both with the original HALOE data (yellow curve) and with the degraded HALOE data (black curve). It is obvious that the amplitude of the annual cycle in HALOE data is much larger than in the MIPAS data (green and red curve). The reason is roughly this: in the case of MIPAS the unknown variable in the retrieval is not the mixing ratio of H_2O but its logarithm. Thus the Jacobian of the radiative transfer model depends directly on the mixing ratio (vmr) of water vapour, even if radiative transfer is linear with respect to vmr. For larger H_2O abundances the Jacobian is larger and thus the weight of the constraint term in the retrieval is smaller and the altitude resolution is better. From this follows that MIPAS resolves the hygropause better in the wet season than in the dry season. This leads to the asymmetric distortion of the annual cycle, seen when comparing the black and the yellow curve in Fig. 2. Application of the season-dependent MIPAS averaging kernels to HALOE data as described above leads to a HALOE time series which is almost perfectly comparable to that of MIPAS. This pronounced effect proves that the direct analysis of MIPAS H_2O time series without consideration of averaging kernels is prone to false conclusions.

3.3 Debiasing

The MIPAS-HALOE overlap period from July 2002 to August 2005 allows for debiasing of MIPAS with respect to HALOE. This debiasing was performed independently for the MIPAS HR and RR data, because these two data sets rely on different processing schemes and thus could theoretically have different characteristics. By the independent debiasing of each of the two MIPAS data sets with respect to HALOE, also biases between both the MIPAS data sets are removed implicitly. These, however, were found to be small, anyway.

Three different approaches to determine the bias were tested, one relying on coincident measurements, the other relying on latitudinal mean values, and the third minimizing the root mean squares difference of the MIPAS and HALOE time series during the overlap period. The third method proved most robust and was finally selected. Debiasing was performed separately for each 10° latitude bin between 80° N and 80° S and for each altitude of the MIPAS vertical grid. An example is shown in Fig. 2 (red curve). The merged time series used within our further analysis is represented as black and red line. Within the overlap period a weighted average of HALOE and MIPAS data has been used.

The MIPAS instrument stability has been assessed (M. Kiefer, personal communication, 2015). A possible drift due to detector-aging and resulting changes of its non-linear response was estimated at approximately $-0.05\,\mathrm{ppmv\,decade^{-1}}$ in the relevant altitude range.

4 Regression analysis

In order to better understand the temporal variation of H_2O in the lower stratosphere, a multilinear regression analysis of the time series was performed for each altitude/latitude bin. The regression model proposed by von Clarmann et al. (2010) and extended by Stiller et al. (2012b) was used for this purpose. It optionally considers the use of the full data error covariance matrix and represents the local volume mixing ratio of water vapour as a function of time using as fit variables a constant term, a linear trend, amplitudes of various harmonic oscillations and user defined proxies. Piecewise linear trends as derived by the cumulative sum method following Reinsel (2002) or Jones et al. (2009) were tried but finally not considered because they merely help to describe but not to explain the temporal variation. For each harmonic both the coefficients of the sine and the cosine term are fitted, which together control both the phase and the amplitude of the harmonic. The correlated part of the error is attributed to variations not described in the regression model. The correlation coefficients of this model error term are obtained from the residuals of a first iteration where only the standard errors of the monthly mean mixing ratios were considered as data errors. The amplitude of this additional error term was adjusted iteratively to comply with χ^2 statistics (von Clarmann et al., 2010).

4.1 The standard regression

Besides the constant and linear term, the annual cycle and its first three overtones (wavenumbers two, three, and four waves per year) were considered. Wavenumber two represents the semi-annual oscillations, and wavenumbers two to four help to better model the annual cycle when it is not perfectly harmonic. The following proxies were considered:

The quasi-biennial oscillation (QBO) was parametrized using Singapore winds at 30 and 50 hPa, as obtained from the Institut für Meteorologie of the Freie Universität Berlin, (http://www.geo.fu-berlin.de/met/ag/strat/produkte/qbo/index/html). Between the winds at these pressure levels, there is a phase shift of approximately $\frac{\pi}{2}$. Thus, fitting coefficients of both of these gives access to the approximate phase and amplitude of the QBO signal (c.f., e.g. Kyrölä et al., 2004).

For the El Niño Southern Oscillation (ENSO) signal, the Multivariate ENSO Index (MEI) (http://www.esrl.noaa.gov/psd/enso/mei/index.html) was used as a proxy. Since this data set refers to a tropical surface pressure level, a time lag was considered to make the proxy representative for the stratospheric latitudes and altitudes considered here. To estimate the time lag, stratospheric mean age of air (AoA) data from Stiller et al. (2012b) were used.

In the fitted time series there are pronounced systematic residuals. Some of them are related to an apparent discontinuity in the water vapour abundance in 2001, the well known water vapour drop (Randel et al., 2006; Urban et al., 2014) but the fits are unsatisfactory in the entire period before 2007. The residual time series appears to be dominated by a systematic harmonic feature of a period length of about eleven years. Figure 3 shows the fit of the time series at 17 km altitude in the latitude bin 0–10° S as an example.

4.2 Consideration of the solar cycle

The fit residuals obtained by the regression analysis described in the previous section resemble a harmonic with a period of about 11 years, with strong H_2O decreases in 1994 and 2001. Thus it suggests itself to also consider the solar cycle in the regression model. Two approaches have been tried:

Approach 1: The solar cycle was modeled by a harmonic of 127 months with an overtone of 63 months (cf. Cunnold et al., 2004). Fitting of the related sine and cosine coefficients gave access to the amplitude and phase of the solar signal. Consideration of the solar term improves the fits within 60° S–60° N in 92 % of the altitude/latitude bins (Fig. 4). The improvement is most pronounced at altitudes around 25 km and reaches 20–30 % in some altitude/latitude bins. The time series at 0–10° S, 17 km altitude is shown as an example how the new regression model fits the time series (Fig. 5). While both the H_2O minimum in 1994 and the so-called millenium drop in 2001 are still visible in the residual data and still beg for explanation, the majority of the systematic residuals have disappeared and the general shape of the time series is nicely reproduced by the regression model. This result suggests that the solar cycle might indeed partially control lower stratospheric water vapour.

Approach 2: Alternatively to the treatment with harmonics, the solar cycle has been fitted using the radio flux index at a wavelength of 10.7 cm (F10.7) as a proxy. This index, which is available via the Solar and Heliospheric Observatory (SOHO, http://sohowww.nascom.nasa.gov/sdb/ydb/indices_flux_raw/DAILYPLT.ADJ) is proportional to solar activity. Since it is not a priori clear which solar-terrestric processes might control the H_2O content of the stratosphere and where exactly they happen, and how long the processed air travels through the stratosphere before it is observed, the phase shift obtained from Approach 1 (approximation of the solar cycle effect by harmonic functions) has also been applied to the F10.7 proxy. Anti-correlation (lowest water vapour for solar maximum) provided the best results. The improvements over the regression without the solar term are shown in Fig. 6. While the improvements are less extreme in some of the bins, this approach seems to be more adequate for the inner tropical lowermost stratosphere. For 95 % of the bins within 60° S–60° N the fit has been improved compared to the standard approach without solar cycle. The altitude/latitude bin at 0–10° S, 17 km is shown as an example (Fig. 7) In this particular case, the residual due to the millenium drop is much less pronounced than in the case with the regression model using the harmonic representation of the solar cycle effect but still visible.

Both approaches reveal a strong relation between the water vapour abundances and the solar cycle. The correlation is phase-shifted in a sense that lowest water vapour abundances are seen a couple of years after the solar maximum (see Fig. 7 as an example).

The amplitudes of the solar component in the regression model are shown in Fig. 8 for both the harmonic (top panel) and the F10.7 (bottom panel) parametrization. While the amplitudes associated with the harmonic approach are larger, the altitude/latitude distributions of the amplitudes associated with each approach have the same structure. Largest effects are seen around the tropical tropopause region, and smallest in the southern midlatitudinal middle stratosphere.

The propagation of the data errors through the regression model leads to uncertainties of these amplitudes of generally less than 2 % within the tropical pipe and less than 5 % outside. Fit residuals, however, are not compliant with χ^2-statistics, indicating that the regression model even with the solar term included is less than perfect and does not fully describe the entire variation of stratospheric H_2O. Analysis of the fit residuals and consideration of resulting estimates of correlated model errors suggests an uncertainty in the order of 15 to 50 % over a larger part of the altitude/latitude range, with highest and contiguous significance (15–25 % relative error of the amplitude) in the tropical tropopause range. This provides good confidence in the results.

The phase shift of the solar signal (Fig. 9) is an interesting result in itself because it helps to determine where in the atmosphere the solar-terrestric processes controlling the stratospheric H_2O content might take place. The phase shift – which, for all altitude/latitude bins, represents a delay of the negative response of water vapour to the original solar cycle – is about 40 months at about 18 km altitude and 45 to 50 months at about 22 km altitude in the inner tropics, which implies a gradient of the shift of half a year per 4 km altitude. Mean ages of stratospheric air as reported by Stiller et al. (2012b) are about two and a half and three years at these altitudes, respectively, leading to a gradient that is roughly the same. This suggests that the solar effect is not a local one but that the shift might be caused by transport processes of a signal generated near the tropical tropopause. Admittedly, for higher altitudes and latitudes, this effect is much less clear and thus recalcitrant with respect to an easy explanation. In particular, after having reached a maximum in the lower stratosphere (green/yellow belt in Fig. 9), the phase shift becomes smaller again for higher altitudes and latitudes. Further, the fact that the phase shift is larger than the age of air in the lowermost stratosphere suggests that the effect itself must have an inherent time lag. This inherent time lag can be estimated from the difference of the phase shift of the solar signal and the age of stratospheric air as derived in Stiller et al. (2012b), assuming that the solar perturbation is transported from the tropical tropopause region into the stratosphere by the stratospheric residual circulation. Indeed, Fig. 10 demonstrates that within 50° N/S and between about 15 and 23 km in the tropics (18 km in the extra-tropics) the inherent time lag is almost constant and amounts to roughly 25 months (extrema are 15 and 30 months). Beyond this altitude/latitude range the difference between solar signal phase shift and age of air is negative and decreases further with altitude and latitude. This hints at different processes governing the solar cycle response of water vapour at higher altitudes.

4.3 Implication for the linear trends and other regression parameters

Inclusion of a solar cycle by either approach discussed in Sect. 4.2 has improved the fit of the regression model to the measured H_2O time series. The systematic residuals observed when the solar component had not been considered largely disappeared when a solar cycle signal was considered. When the F10.7 proxy was used, even the millenium drop was – coincidentally or not – modelled much better. Regardless if a causal relation between solar activity and the lower stratospheric H_2O distribution is claimed or not, any missing descriptive term in an incomplete regression model causes residuals which are aliased onto other parameters in the fit. In the case discussed here, inclusion of the solar cycle terms leads to much more negative water vapour trends and in some cases even changes the sign of the trend (Fig. 11). In the standard regression model stratospheric water vapour abundances increase or decrease by less than 0.2 ppmv decade^{-1} nearly everywhere. In particular, a contiguous increase in the lowermost stratosphere in the order of 0.1–0.2 ppmv decade^{-1} is seen. When the solar cycle is considered, stratospheric water vapour decreases everywhere, and stronger than by –0.1 ppmv decade^{-1} at most latitudes and altitudes. This indicates that, even if one does not believe the solar cycle effect in explanatory terms, it still is important in descriptive terms in order to avoid artefacts caused by the related systematic residuals. Systematic effects on the annual and semiannual cycles as well as QBO and ENSO amplitudes are much less pronounced.

5 Discussion

The analysis of the merged MIPAS-HALOE time series by multivariate linear regression including a solar cycle proxy as described above suggests that a solar signal is imprinted on the water vapour abundance entering the stratosphere at the tropical tropopause, and this signal then is transported to the middle stratosphere via the Brewer–Dobson circulation. The signal vanishes in the middle stratosphere. The solar signal in the water vapour time series is phase-shifted anti-correlated to the solar cycle, i.e. lowest water vapour after solar maximum is found. The phase shift consists of two components: the first component is an inherent time lag of about 25 months; the second component results from transport times in the stratosphere by the Brewer–Dobson circulation as given by the mean age of air.

Two obvious candidates to explain a solar signal in lower stratospheric water vapour are methane oxidation and the import of water vapour through the tropical tropopause into the stratosphere.

The photochemical oxidation of methane is an important contribution to the stratospheric water vapour budget (le Texier et al., 1988). However, the efficiency of the conversion increases with altitude, and this is opposite to the solar cycle variation observed here (see Fig. 8). The variations of methane in the tropical lower stratosphere are very small (less than 0.1 ppmv, not shown here) and not sufficient to explain the observed variation in lower stratospheric water vapour.

The import of water vapour from the troposphere into the stratosphere is to a first order regulated by the tropical tropopause temperature which implies that any mechanism leading to solar cycle influence on the tropopause temperatures could explain the solar cycle signal in water vapour.

There are different studies that analyze the influence of the solar cycle onto the tropical tropopause temperature with different results: Krüger et al. (2008) look at the NH winter time, when the lowest temperatures and water vapour entry values are observed in the lower stratosphere. They use a trajectory model fed with input from ECMWF. In a zonal average they find 0.2 K higher cold point temperatures during solar maximum as compared to solar minimum which would contradict our findings. However, over the Western Pacific, where most of the air experiences its final dehydration, they find a stronger negative temperature anomaly in the order of 1 K for solar maximum and a respective positive temperature anomaly for the solar minimum. By estimation of the saturation vapour pressure over ice we find that a coldpoint temperature amplitude of this magnitude could explain about half of the amplitude of the tropical H_2O variation seen by MIPAS. Regression analysis of observed water vapour variations and approximate cold point temperatures from an ensemble of observational data sets (Schieferdecker, 2015) suggest that even two thirds of the observed solar component of the vapour variability can be explained by a 2 K solar temperature variation.

Frame and Gray (2010) report higher temperatures during solar max right above the tropical tropopause and lower temperatures right below the tropopause. However, there is no obvious response at the tropopause itself.

Chiodo et al. (2014) use Whole Atmosphere Community Model (WACCM) 3.5 simulations from 1960–2004 to study the solar cycle influence. The analysis indicates that there is a positive correlation between solar cycle and stratospheric temperature; however, large parts can be attributed to the alignment of the solar cycle with Pinatubo and El Chichon eruptions. They conclude that it is very difficult to unambiguously assign the variability to the solar cycle. Typically they find a lag of 1 year between the lower stratospheric temperature response and the solar forcing (averaged over 25° S–25° N). This is different from our results where the time lag is much larger. Chiodo et al. (2014) can extract a robust signal only above 10 hPa while below the ambiguity between volcanic influence and solar cycle is too pronounced.

Both the “top-down” solar influence based on solar heating of the stratosphere and the “bottom-up” mechanism (based on solar heating of the sea surface and dynamically coupled air–sea interaction) strengthen the tropical convection and produce an amplified sea surface temperature (SST), precipitation, and cloud response in the tropical Pacific to a relatively small solar forcing (see Gray et al., 2010, and references therein). Assuming that the cause of the solar signal seen in water vapour comes from the ocean Deckert and Dameris (2008a, b) provide an explanation how the signal is transported from the ocean to the lower stratosphere. Higher sea surface temperatures amplify deep convection locally. The latent heat release from the convection induces pressure perturbations which in turn manifest themselves in the excitation of quasi-stationary planetary waves. These move upwards through the easterly winds, dissipate, but are still strong enough to induce a strengthening of the upwelling. This happens during summer (June to September in the Northern Hemisphere and between December and March in the Southern Hemisphere), i.e. not during the times when the Brewer–Dobson-circulation is strongest, and at a different season than that addressed by Krüger et al. (2008). This effect is discussed with respect to climate change but their arguments could easily be applied to solar-cycle-induced changes of the sea surface temperature as well.

According to White et al. (1997) globally averaged SST anomalies show highest correlations with solar activity with a phase shift of 1–2 years. White and Liu (2008) found that the eastern tropical Pacific warm phase of the 11 year cycle lagged the peak solar forcing by 1–3 years which both is in good agreement to the inherent lag identified in the solar signal in the water vapour time series.

Regarding the water vapour trends, there was agreement until recently that water vapour in the lower stratosphere has increased over the previous decades (Oltmans et al., 2000; Rosenlof et al., 2001; Hurst et al., 2011).

Only recently, Hegglin et al. (2014) analyzed H_2O trends of data records obtained with various space-borne limb-sounding instruments and found negative trends. Data merging was performed using the Canadian Middle Atmosphere Model 30 (CMAM30) (Scinocca et al., 2008) as a transfer standard. The different temporal coverage of their and our analysis is a major obstacle for a direct comparison. Nevertheless, they found negative trends of water vapour in the lower stratosphere in the order of 10 % over 22 years which is somewhat larger than our values, and they attribute this change mainly to an intensification of the shallow branch of the Brewer–Dobson circulation.

The analysis performed by Dessler et al. (2014) is mainly based on the MLS time series and constructed water vapour abundances applying a trajectory model on reanalyses. They found that tropical lower stratospheric water vapour can be described by a multivariate linear regression including the troposphere temperature at 500 hPa, a QBO proxy and a proxy of the Brewer–Dobson circulation only. With this parameterization no significant linear trend remains.

The findings by Hegglin et al. (2014) and Dessler et al. (2014) neither confirm nor refute our findings. The reasons are these: first, we find it only natural that trends, which by their nature are a descriptive rather than an explaining quantity, are found different, depending on which explaining fit parameters are used. Second, the solar cycle might also act upon other atmospheric quantities, which in turn are correlated

Title Page
Abstract Introduction
Conclusions References
Tables Figures
◀| |▶
◀ ▶
Back Close
Full Screen / Esc
Printer-friendly Version
Interactive Discussion

with the variation of water vapour. In particular, solar influence on both the tropospheric temperature and the Brewer–Dobson circulation were identified (see Gray et al., 2010) which implies that the parameterisation chosen by Dessler et al. (2014) has implicitly included a possible solar signal in water vapour.

6 Conclusions

A parametric fit of a 20 year time series of lower stratospheric water vapour based on a merged MIPAS–HALOE dataset is improved by inclusion of a solar cycle term. The water vapour data records within 60° S–60° N and 15 to 30 km are best described by including a solar cycle proxy implying a phase-shifted anti-correlation between water vapour abundances and solar radiation (i.e. lowest water vapour after solar maximum). Within the lower stratosphere this phase shift is composed of an almost constant inherent time lag of about 25 months and a variable delay following the age of stratospheric air. Amplitudes of the solar signal in the water vapour time series are largest near the tropical tropopause (up to 0.35 ppmv) and decrease with altitude and latitude. The behaviour of both the amplitudes and the phase shifts indicate that the solar signal is imprinted on the water vapour entering the stratosphere through the tropical tropopause, and is, thus, a consequence of tropopause temperatures influenced by the solar cycle. The response of lower stratospheric water vapour to the solar cycle suggests that tropopause temperatures relevant for the dehydration of air are lowest about two years after solar maximum.

Inclusion of the solar cycle term in the multivariate linear regression of the water vapour time series has another important consequence: the linear term, interpretable as a trend over the two decades of observation, becomes considerably more negative after inclusion of the solar cycle proxy and in the lowermost stratosphere the “trend” even changes sign from slightly positive without the solar proxy term to significantly negative. Thus, including the solar cycle term as additional proxy of a driver that rules stratospheric water vapour has the potential to resolve the water vapour conundrum of increasing water vapour abundances despite constant or even slightly decreasing tropopause temperatures (Rosenlof and Reid, 2008; Randel et al., 2006; Zhou et al., 2001).

A robust causal[1] attribution of the lower stratospheric water vapour fluctuations to solar effects is admittedly a challenge because of the small temporal coverage of the time series, which includes less than two solar cycles. But at least it can be said that in descriptive terms the lower stratospheric water vapour time series shows a signal which can be well modelled by a solar cycle signal and whose disregard can affect water vapour trend estimation. Consideration of other H_2O data sources beyond MIPAS and HALOE suggests itself as obvious follow-up activity.

Acknowledgements. The provision of MIPAS level-1b data by ESA is gratefully acknowledged. HALOE data were downloaded from http://haloe.gats-inc.com/download/index.php. We acknowledge the HALOE team for their efforts with regard to the instrument operations and the generation and characterisation of the HALOE data set. T. Schieferdecker and S. Lossow were funded by the DFG Research Unit "Stratospheric Change and its Role for Climate Prediction" (SHARP) under contracts STI 210/9-1 and STI 210/9-2. Development of water vapour data retrieval was partly funded by the German Federal Ministry of Education and Research (BMBF) under contract no. 50EE0901. We acknowledge support by Deutsche Forschungsgemeinschaft and the Open Access Publishing Fund of Karlsruhe Institute of Technology.

The article processing charges for this open-access publication were covered by a Research Centre of the Helmholtz Association.

---

[1] It is a general truism that statistical coincidence never assures a causal relation but we can neither imagine that Earth's atmosphere affects solar activity or that both lower stratospheric water vapour and solar activity are controlled by a third driver. Thus we consider pure coincidence as the only serious alternative hypothesis.

References

Chiodo, G., Marsh, D. R., Garcia-Herrera, R., Calvo, N., and García, J. A.: On the detection of the solar signal in the tropical stratosphere, Atmos. Chem. Phys., 14, 5251–5269, doi:10.5194/acp-14-5251-2014, 2014. 12367

Connor, B. J., Siskind, D. E., Tsou, J. J., Parrish, A., and Remsberg, E. E.: Ground-based microwave observations of ozone in the upper stratosphere and mesosphere, J. Geophys. Res., 99, 16757–16770, doi:10.1029/94JD01153, 1994. 12358

Corti, T., Luo, B. P., de Reus, M., Brunner, D., Cairo, F., Mahoney, M. J., Martucci, G., Matthey, R., Mitev, V., Silva dos Santos, F. H., Schiller, C., Shur, G., Sitnikov, N. M., Spelten, N., Vössing, H. J., Borrmann, S., and Peter, T.: Unprecedented evidence for deep convection hydrating the tropical stratosphere, Geophys. Res. Lett., 35, L10810, doi:10.1029/2008GL033641, 2008. 12355

Cunnold, D. M., Yang, E.-S., Newchurch, M. J., Reinsel, G. C., Zawodny, J. M., and Russell III, J. M.: Comment on “Enhanced upper stratospheric ozone: Sign of recovery or solar cycle effect?” by W. Steinbrecht et al., J. Geophys. Res., 109, D14305, doi:10.1029/2004JD004826, 2004. 12362

Deckert, R. and Dameris, M.: Higher tropical SSTs strengthen the tropical upwelling via deep convection, Geophys. Res. Lett., 35, L10813, doi:10.1029/2008GL033719, 2008a. 12367

Deckert, R. and Dameris, M.: From ocean to stratosphere, Science, 322, 53–55, doi:10.1126/science.1163709, 2008b. 12367

Dessler, A. E. and Kim, H.: Determination of the amount of water vapor entering the stratosphere based on Halogen Occultation Experiment, J. Geophys. Res., 104, 30605–30607, 1999. 12357

Dessler, A. E., Schoeberl, M. R., Wand, T., Davis, S. M., Rosenlof, K. H., and Vernier, J.: Variations of stratospheric water vapor over the past three decades, J. Geophys. Res., 119, 12588–12598, doi:10.1002/2014JD021712, 2014. 12368, 12369

Fischer, H., Birk, M., Blom, C., Carli, B., Carlotti, M., von Clarmann, T., Delbouille, L., Dudhia, A., Ehhalt, D., Endemann, M., Flaud, J. M., Gessner, R., Kleinert, A., Koopman, R., Langen, J., López-Puertas, M., Mosner, P., Nett, H., Oelhaf, H., Perron, G., Remedios, J., Ridolfi, M., Stiller, G., and Zander, R.: MIPAS: an instrument for atmospheric and climate research, Atmos. Chem. Phys., 8, 2151–2188, doi:10.5194/acp-8-2151-2008, 2008. 12355, 12356, 12357

Frame, T. H. A. and Gray, L. J.: The 11 year solar cycle in ERA-40 data: an update to 2008, J. Climate, 23, 2213–2222, doi:10.1175/2009JCLI3150.1, 2010. 12367

Froidevaux, L., Anderson, J., Wang, H.-J., Fuller, R. A., Schwartz, M. J., Santee, M. L., Livesey, N. J., Pumphrey, H. C., Bernath, P. F., Russell III, J. M., and McCormick, M. P.: Global OZone Chemistry And Related Datasets for the Stratosphere (GOZCARDS): methodology and sample results with a focus on HCl, H_2O, and O_3, Atmos. Chem. Phys. Discuss., 15, 5849–5957, doi:10.5194/acpd-15-5849-2015, 2015. 12356

Fueglistaler, S.: Stepwise changes in stratospheric water vapor?, J. Geophys. Res., 117, D13302, doi:10.1029/2012JD017582, 2012. 12355

Fueglistaler, S., Bonazzola, M., Haynes, P. H., and Peter, T.: Stratospheric water vapor predicted from the Lagrangian temperature history of air entering the stratosphere in the tropics, J. Geophys. Res., 110, D08107, doi:10.1029/2004JD005516, 2005. 12355

Fueglistaler, S., Dessler, A. E., Dunkerton, T. J., Folkins, I., Fu, Q., and Mote, P. W.: Tropical tropopause layer, Rev. Geophys., 47, RG1004, doi:10.1029/2008RG000267, 2009. 12355

Fueglistaler, S., Liu, Y. S., Flannaghan, T. J., Haynes, P. H., Dee, D. P., Read, W. J., Remsberg, E. E., Thomason, L. W., Hurst, D. F., Lanzante, J. R., and Bernath, P. F.: The relation between atmospheric humidity and temperature trends for stratospheric water, J. Geophys. Res., 118, 1052–1074, doi:10.1002/jgrd.50157, 2013. 12355

Gray, L. J., Beer, J., Geller, M., Haigh, J. D., Lockwood, M., Matthes, K., Cubasch, U., Fleitmann, D., Harrison, G., Hood, L., Luterbacher, J., Meehl, G. A., Shindell, D., van Geel, B., and White, W.: Solar influences on climate, Rev. Geophys., 48, RG4001, doi:10.1029/2009RG000282, 2010. 12367, 12369

Harries, J. E., Russell III, J. M., Tuck, A. F., Gordley, L. L., Purcell, P., Stone, K., Bevilacqua, R. M., Gunson, M., Nedoluha, G., and Traub, W. A.: Validation of measurements of water vapor from the Halogen Occultation Experiment (HALOE), J. Geophys. Res., 101, 205–210, 1996. 12357

Hegglin, M. I., Tegtmeier, S., Anderson, J., Froidevaux, L., Fuller, R., Funke, B., Jones, A., Lingenfelser, G., Lumpe, J., Pendlebury, D., Remsberg, E., Rozanov, A., Toohey, M., Urban, J., von Clarmann, T., Walker, K. A., Wang, R., and Weigel, K.: SPARC Data Initiative: comparison of water vapor climatologies from international satellite limb sounders, J. Geophys. Res. Atmos., 118, 824–811, doi:10.1002/jgrd.50752, 2013. 12356

Hegglin, M. I., Plummer, D. A., Shepherd, T. G., Scinocca, J. F., Anderson, J., Froidevaux, L., Funke, B., Hurst, D., Rozanov, A., Urban, J., von Clarmann, T., Walker, K. A., Wang, H. J., Tegtmeier, S., and Weigel, K.: Vertical structure of stratospheric water vapour trends derived from merged satellite data, Nat. Geosci., 7, 768–776, doi:10.1038/ngeo2236, 2014. 12355, 12368

Hervig, M. E., Russell III, J. M., Gordley, L. L., Daniels, J., Drayson, S. R., and Park, J. H.: Aerosol effects and corrections in the Halogen Occultation Experiment, J. Geophys. Res., 100, 1067–1079, 1995. 12356

Holton, J. R. and Gettelmann, A.: Horizontal transport and the dehydration of the stratosphere, Geophys. Res. Lett., 28, 2799–2802, 2001. 12355

Hurst, D. F., Oltmans, S. J., Vömel, H., Rosenlof, K. H., Davis, S. M., Ray, E. A., Hall, E. G., and Jordan, A. F.: Stratospheric water vapor trends over Boulder, Colorado: analysis of the 30 year Boulder record, J. Geophys. Res., 116, D02306, doi:10.1029/2010JD015065, 2011. 12355, 12368

Jones, A., Urban, J., Murtagh, D. P., Eriksson, P., Brohede, S., Haley, C., Degenstein, D., Bourassa, A., von Savigny, C., Sonkaew, T., Rozanov, A., Bovensmann, H., and Burrows, J.: Evolution of stratospheric ozone and water vapour time series studied with satellite measurements, Atmos. Chem. Phys., 9, 6055–6075, doi:10.5194/acp-9-6055-2009, 2009. 12360

Kiehl, J. T. and Trenberth, K. E.: Earth's annual global mean energy budget, B. Am. Meteorol. Soc., 78, 197–208, 1997. 12354

Kley, D., Russell III, J. M., and Phillips, C. (Eds.): Stratospheric Processes and their Role in Climate (SPARC) – assessment of upper tropospheric and stratospheric water vapour, WCRP No. 113, WMO/TD - No. 1043, SPARC Report No.2, WMO/ICSU/IOC, Paris, 2000. 12356

Krüger, K., Tegtmeier, S., and Rex, M.: Long-term climatology of air mass transport through the Tropical Tropopause Layer (TTL) during NH winter, Atmos. Chem. Phys., 8, 813–823, doi:10.5194/acp-8-813-2008, 2008. 12366, 12367

Kyrölä, E., Tamminen, J., Leppelmeier, G. W., Sofieva, V., Hassinen, S., Bertaux, J. L., Hauchecorne, A., Dalaudier, F., Cot, C., Korablev, O., Fanton d'Andon, O., Barrot, G., Mangin, A., Théodore, B., Guirlet, M., Etanchaud, F., Snoeij, P., Koopman, R., Saavedra, L., Fraisse, R., Fussen, D., and Vanhellemont, F.: GOMOS on Envisat: an overview, Adv. Space Res., 33, 1020–1028, doi:10.1016/S0273-1177(03)00590-8, 2004. 12361

le Texier, H., Solomon, S., and Garcia, R. R.: The role of molecular hydrogen and methane oxidation in the water vapour budget of the stratosphere, Q. J. Roy. Meteor. Soc., 114, 281–295, 1988. 12366

Manabe, S. and Strickler, R. F.: Thermal equilibrium of the atmosphere with a convective adjustment, J. Atmos. Sci., 21, 361–385, 1964. 12354

Milz, M., von Clarmann, T., Fischer, H., Glatthor, N., Grabowski, U., Höpfner, M., Kellmann, S., Kiefer, M., Linden, A., Mengistu Tsidu, G., Steck, T., Stiller, G. P., Funke, B., López-Puertas, M., and Koukouli, M. E.: Water vapor distributions measured with the Michelson Interferometer for Passive Atmospheric Sounding on board Envisat (MIPAS/Envisat), J. Geophys. Res., 110, D24307, doi:10.1029/2005JD005973, 2005. 12357

Milz, M., Clarmann, T. v., Bernath, P., Boone, C., Buehler, S. A., Chauhan, S., Deuber, B., Feist, D. G., Funke, B., Glatthor, N., Grabowski, U., Griesfeller, A., Haefele, A., Höpfner, M., Kämpfer, N., Kellmann, S., Linden, A., Müller, S., Nakajima, H., Oelhaf, H., Remsberg, E., Rohs, S., Russell III, J. M., Schiller, C., Stiller, G. P., Sugita, T., Tanaka, T., Vömel, H., Walker, K., Wetzel, G., Yokota, T., Yushkov, V., and Zhang, G.: Validation of water vapour profiles (version 13) retrieved by the IMK/IAA scientific retrieval processor based on full resolution spectra measured by MIPAS on board Envisat, Atmos. Meas. Tech., 2, 379–399, doi:10.5194/amt-2-379-2009, 2009. 12357

Oltmans, S. J., Vömel, H., Hofmann, D. J., Rosenlof, K. H., and Kley, D.: The increase in stratospheric water vapor from ballooneborne, frostpoint hygrometer measurements at Washington, D. C., and Boulder, Colorado, Geophys. Res. Lett., 27, 3453–3456, 2000. 12368

Randel, W. J., Wu, F., Vömel, H., Nedoluha, G. E., and Forster, P.: Decreases in stratospheric water vapor after 2001: links to changes in the tropical tropopause and the Brewer–Dobson circulation, J. Geophys. Res., 111, D12312, doi:10.1029/2005JD006744, 2006. 12355, 12361, 12370

Reinsel, G. C.: Trend analysis of upper stratospheric Umkehr ozone data for evidence of turnaround, Geophys. Res. Lett., 29, 1451, doi:10.1029/2002GL014716, 2002. 12360

Riese, M., Ploeger, F., Rap, A., Vogel, B., Konopka, P., Dameris, M., and Forster, P.: Impact of uncertainties of atmospheric mixing on simulated UTLS composition and related radiative effects, J. Geophys. Res., 117, D16305, doi:10.1029/2012JD017751, 2012. 12355

Rodgers, C. D.: Inverse Methods for Atmospheric Sounding: Theory and Practice, vol. 2 of Series on Atmospheric, Oceanic and Planetary Physics, edited by: F. W. Taylor, World Scientific, Singapore, New Jersey, London, Hong Kong, 2000. 12358

Rosenlof, K. H. and Reid, G. C.: Trends in the temperature and water vapor content of the tropical lower stratosphere: sea surface connection, J. Geophys. Res., 113, D06107, doi:10.1029/2007JD009109, 2008. 12355, 12370

Rosenlof, K. H., Oltmans, S. J., Kley, D., Russell III, J. M., Chiou, E.-W., Chu, W. P., Johnson, D. G., Kelly, K. K., Michelsen, H. A., Nedoluha, G. E., Remsberg, E. E., Toon, G. C., and McCormick, M. P.: Stratospheric water vapor increases over the past half-century, Geophys. Res. Lett., 28, 1195–1198, 2001. 12355, 12368

Russell III, J. M.: HALOE level 2 data description, available at: http://badc.nerc.ac.uk/browse/badc/haloe/doc/haloe_l2.sfdu (last access: 1 June 2014), 1995. 12356

Russell III, J. M., Gordley, L. L., Park, J. H., Drayson, S. R., Hesketh, W. D., Cicerone, R. J., Tuck, A. F., Frederick, J. E., Harries, J. E., and Crutzen, P. J.: The halogen occultation experiment, J. Geophys. Res., 98, 10777–10797, 1993. 12355, 12356

Schieferdecker, T.: Variabilität von Wasserdampf in der unteren und mittleren Stratosphäre auf der Basis von HALOE/UARS und MIPAS/Envisat Beobachtungen, Ph.D. thesis, Karlsruhe Institute of Technology, available at: http://digbib.ubka.uni-karlsruhe.de/volltexte/1000046296 (last access: 10 March 2015), 2015. 12359, 12366

Schiller, C., Grooß, J., Konopka, P., Ploeger, F., Silva dos Santos, F. H., and Spelten, N.: Hydration and dehydration at the tropical tropopause, Atmos. Chem. Phys, 9, 9647–9660, doi:10.5194/acp-9-9647-2009, 2009. 12355

Scinocca, J. F., McFarlane, N. A., Lazare, M., Li, J., and Plummer, D.: Technical Note: The CCCma third generation AGCM and its extension into the middle atmosphere, Atmos. Chem. Phys., 8, 7055–7074, doi:10.5194/acp-8-7055-2008, 2008. 12368

Solomon, S., Rosenlof, K. H., Portmann, R. W., Daniel, J. S., Davis, S. M., Sanford, T. J., and Plattner, G.-K.: Contributions of stratospheric water vapor to decadal changes in the rate of global warming, Science, 327, 1219–1223, doi:10.1126/science.1182488, 2010. 12354

Steele, H. M. and Turco, R. P.: Separation of aerosol and gas components in the Halogen Occultation Experiment and the Stratospheric Aerosol and Gas Experiment (SAGE) II extinction measurements: Implication for SAGE II ozone concentrations and trends, J. Geophys. Res., 102, 19665–19681, 1997. 12357, 12358

Stenke, A. and Grewe, V.: Simulation of stratospheric water vapor trends: impact on stratospheric ozone chemistry, Atmos. Chem. Phys., 5, 1257–1272, doi:10.5194/acp-5-1257-2005, 2005. 12355

Stiller, G. P., Kiefer, M., Eckert, E., von Clarmann, T., Kellmann, S., García-Comas, M., Funke, B., Leblanc, T., Fetzer, E., Froidevaux, L., Gomez, M., Hall, E., Hurst, D., Jordan, A., Kämpfer, N., Lambert, A., McDermid, I. S., McGee, T., Miloshevich, L., Nedoluha, G., Read, W., Schneider, M., Schwartz, M., Straub, C., Toon, G., Twigg, L. W., Walker, K., and Whiteman, D. N.: Validation of MIPAS IMK/IAA temperature, water vapor, and ozone profiles with MOHAVE-2009 campaign measurements, Atmos. Meas. Tech., 5, 289–320, doi:10.5194/amt-5-289-2012, 2012a. 12357, 12358

Stiller, G. P., von Clarmann, T., Haenel, F., Funke, B., Glatthor, N., Grabowski, U., Kellmann, S., Kiefer, M., Linden, A., Lossow, S., and López-Puertas, M.: Observed temporal evolution of global mean age of stratospheric air for the 2002 to 2010 period, Atmos. Chem. Phys., 12, 3311–3331, doi:10.5194/acp-12-3311-2012, 2012b. 12360, 12361, 12364, 12386

Urban, J., Lossow, S., Stiller, G., and Read, W.: Another drop in water vapor, Eos Trans. AGU, 95, 245–246, doi:10.1002/2014EO270001, 2014. 12355, 12361

von Clarmann, T., Glatthor, N., Grabowski, U., Höpfner, M., Kellmann, S., Kiefer, M., Linden, A., Mengistu Tsidu, G., Milz, M., Steck, T., Stiller, G. P., Wang, D. Y., Fischer, H., Funke, B., Gil-López, S., and López-Puertas, M.: Retrieval of temperature and tangent altitude pointing from limb emission spectra recorded from space by the Michelson Interferometer for Passive Atmospheric Sounding (MIPAS), J. Geophys. Res., 108, 4736, doi:10.1029/2003JD003602, 2003. 12357

von Clarmann, T., Höpfner, M., Kellmann, S., Linden, A., Chauhan, S., Funke, B., Grabowski, U., Glatthor, N., Kiefer, M., Schieferdecker, T., Stiller, G. P., and Versick, S.: Retrieval of temperature, H_2O, O_3, HNO_3, CH_4, N_2O, $ClONO_2$ and ClO from MIPAS reduced resolution nominal mode limb emission measurements, Atmos. Meas. Tech., 2, 159–175, doi:10.5194/amt-2-159-2009, 2009. 12357

von Clarmann, T., Stiller, G., Grabowski, U., Eckert, E., and Orphal, J.: Technical Note: Trend estimation from irregularly sampled, correlated data, Atmos. Chem. Phys., 10, 6737–6747, doi:10.5194/acp-10-6737-2010, 2010. 12360, 12361

White, W. B. and Liu, Z.: Resonant response of the quasi-decadal oscillation to the 11 year period signal in the Sun's irradiance, J. Geophys. Res., 113, C01002, doi:10.1029/2006JC004057, 2008. 12368

White, W. B., Lean, J., Cayan, D. R., and Dettinger, M. D.: Response of global upper ocean temperature to changing solar irradiance, J. Geophys. Res., 102, 3255–3266, doi:10.1029/96JC03549, 1997. 12368

Zhou, X.-L., Geller, M. A., and Zhang, M.: Cooling trend of the tropical cold point tropopause temperatures and its implications, J. Geophys. Res, 106, 1511–1522, doi:10.1029/2000JD900472, 2001. 12370

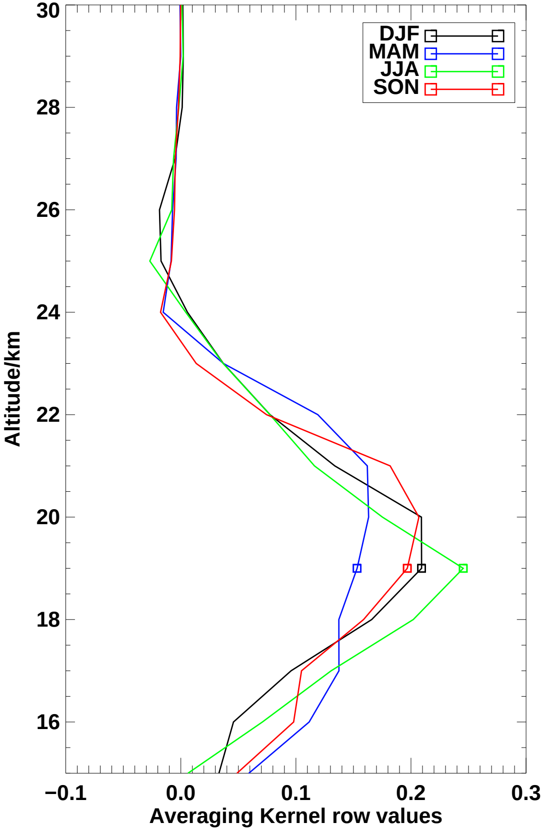

Figure 1. H_2O averaging kernels for December, January, February (DJF, black line), March, April, May (MAM, blue line), July, July, August (JJA, green line) and Septemper, October, November (red line) at 19 km nominal altitude, 0° S–10° S. It should be noted that the kernels refer to log(vmr), not vmr.

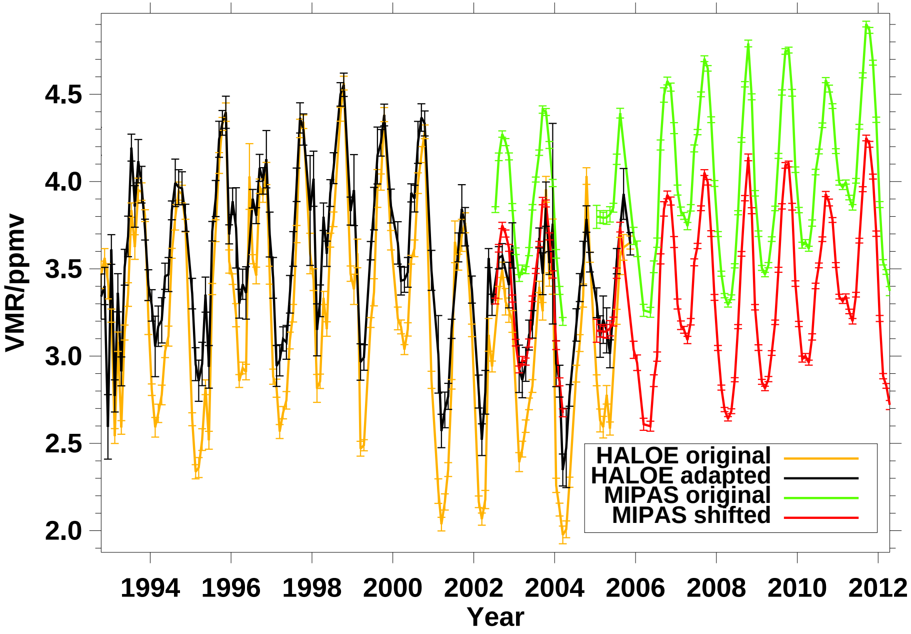

Figure 2. H_2O time series of the original (green) and de-biased (red) MIPAS data, HALOE (yellow) and HALOE after application of the MIPAS averaging kernels (black). The altitude/latitude bin at 20° S–20° N, 17–18 km is shown as an example.

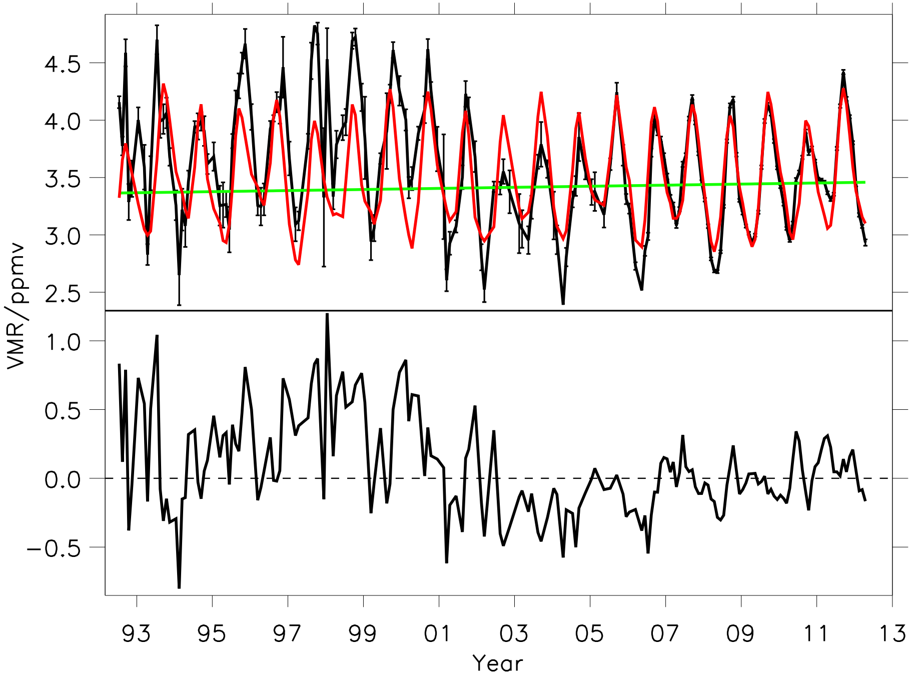

Figure 3. The merged time series (top panel, black curve) with the standard errors of the data (black) and the best fitting standard regression model (top panel, red curve) and the linear term of the regression (green line). In the lower panel the residual time series between the measured data and the fitted regression model is shown. The latitude bin of 0–10° S is shown for an altitude of 17 km as an example. The residual (rms = 0.35 ppmv) appears to have a systematic harmonic component with a period of about 11 years.

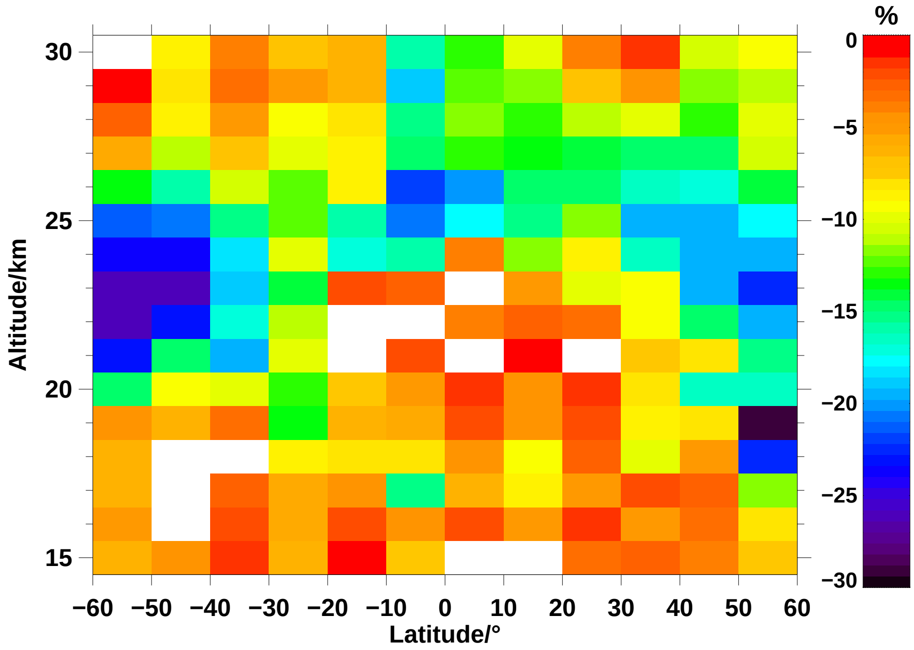

Figure 4. The root mean squares improvement of the fit residual with respect to the standard approach, gained by the inclusion of the solar cycle approximated by harmonic parametrization as described under Approach 1 in Sect. 4.2. White bins are positive values, i.e. deterioration of the fit.

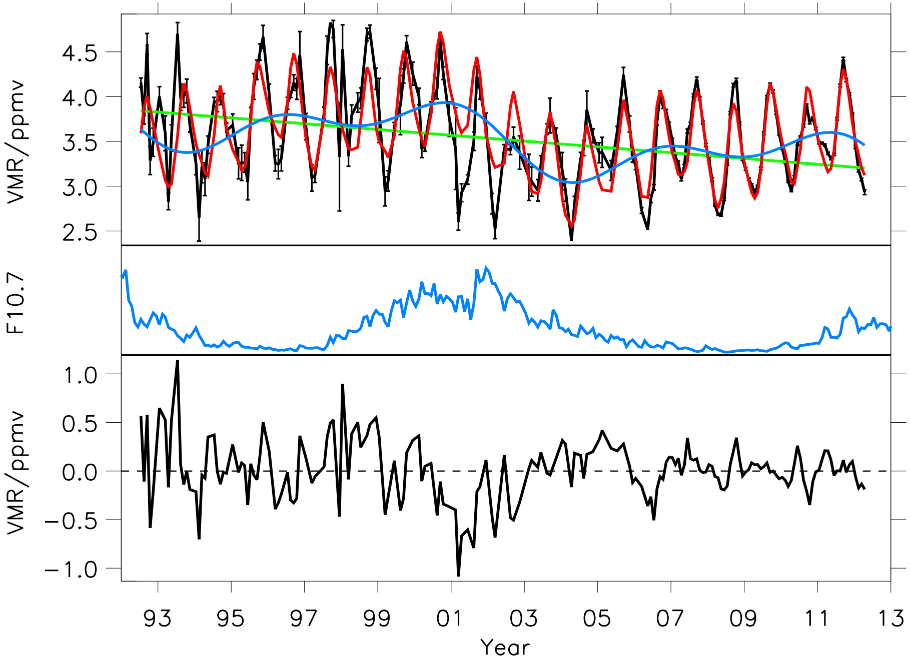

Figure 5. Top panel: fitted regression model with solar cycle approximated by harmonic parametrization as described under Approach 1 in Sect. 4.2. The blue curve is the fitted contribution of these harmonics. The middle panel (blue curve) shows the original solar cycle F10.7 parametrization in arbitrary units. In the lower panel the residual time series between the measured data and the fitted regression model is shown. The rms for this fit is 0.30 ppmv. For further details, see Fig. 3.

Title Page
Abstract | Introduction
Conclusions | References
Tables | Figures
◀| |▶
◀ ▶
Back | Close
Full Screen / Esc
Printer-friendly Version
Interactive Discussion

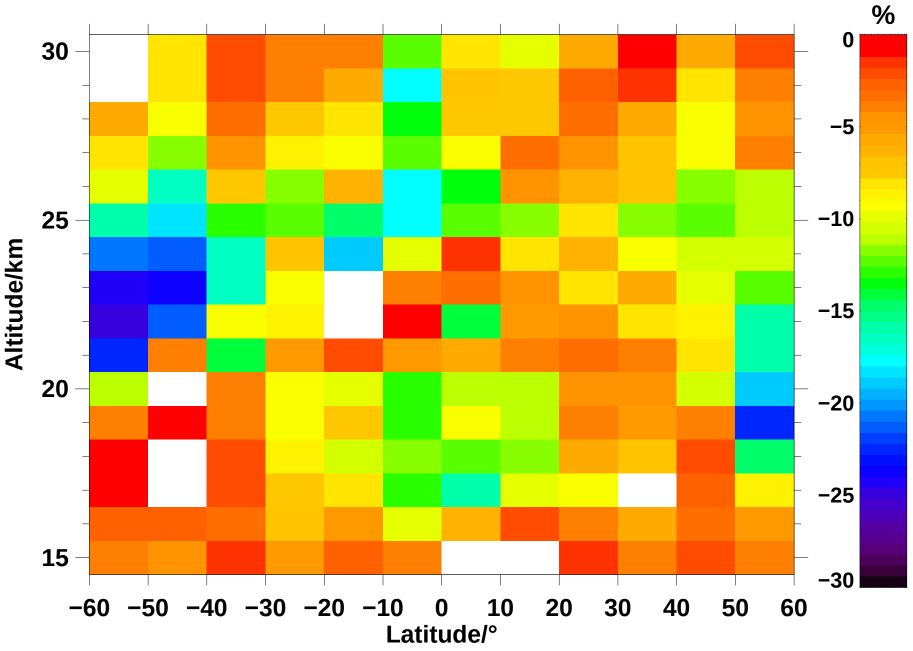

Figure 6. The root mean squares improvement of the fit residual with respect to the standard approach gained by the inclusion of the solar cycle approximated by the F10.7 proxy as described under Approach 2 in Sect. 4.2. White bins are positive values, i.e. deterioration of the fit.

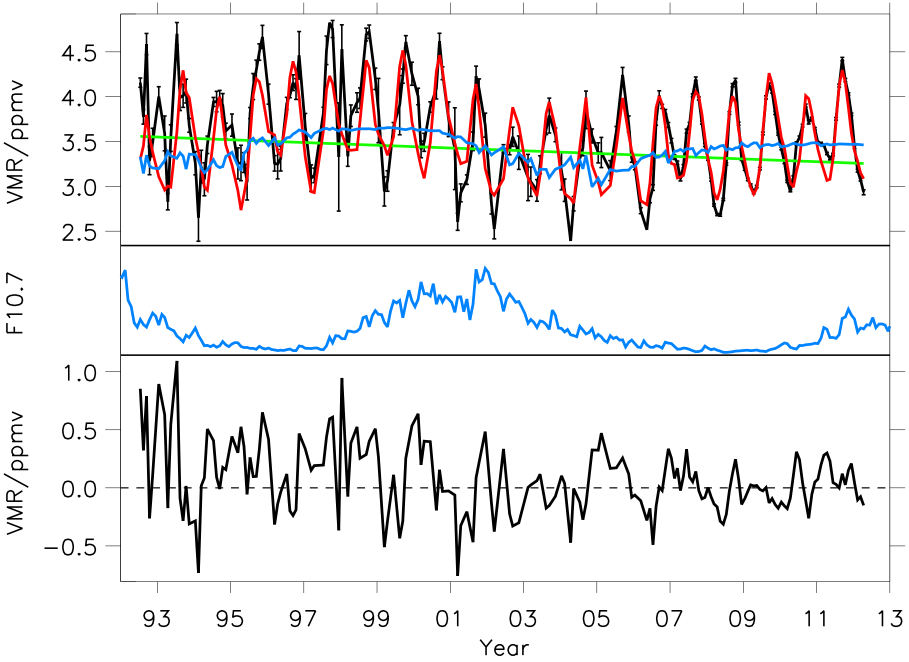

Figure 7. Top panel: fitted regression model with solar cycle approximated by the F10.7 proxy as described under Approach 2 in Sect. 4.2. The blue curve is the fitted solar signal contribution with the F10.7 proxy. The middle panel (blue curve) shows the original solar cycle F10.7 parametrization in arbitrary units. In the lower panel the residual time series between the measured data and the fitted regression model is shown. The rms for this fit is 0.31 ppmv. For further details, see Fig. 3.

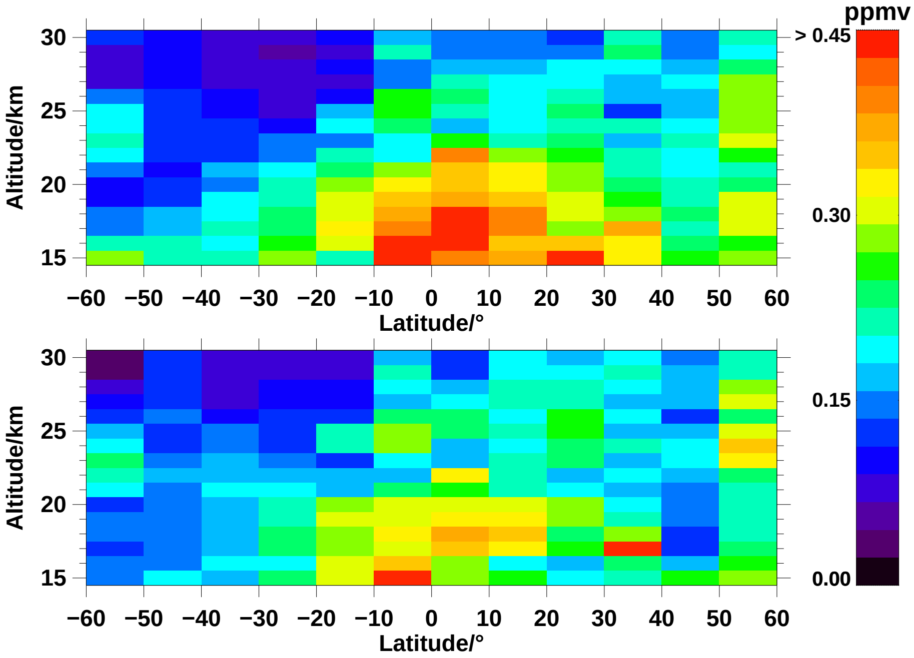

Figure 8. "Quasi-amplitudes" of fitted terms representing the solar cycle in the regression, i.e. the halved differences between the maxima and minima along the time series of these contributions. Top panel: harmonic parametrization; lower panel: F10.7 parametrization.

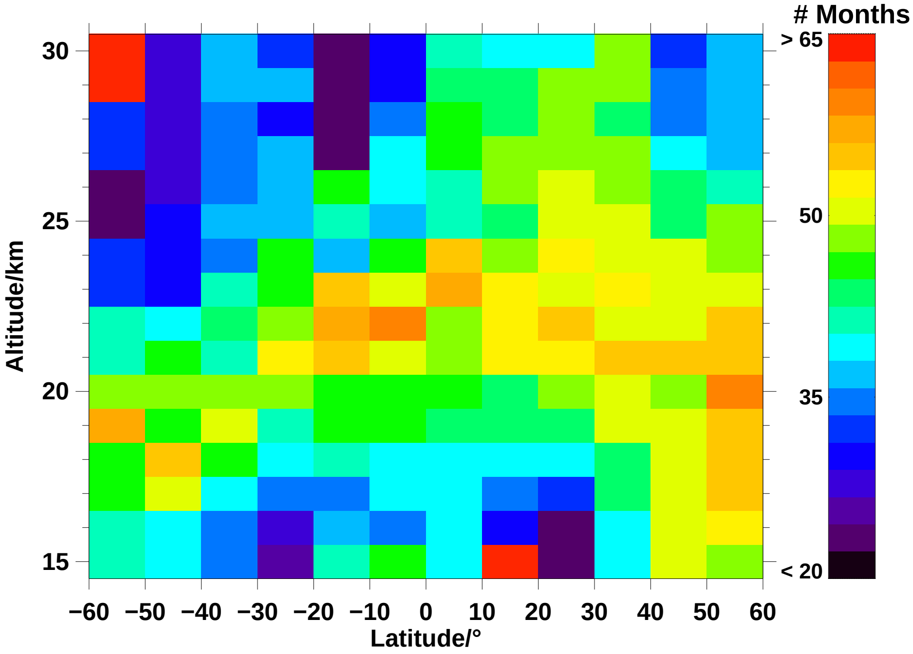

Figure 9. The distribution of the phase shift between the solar maximum and negative water vapour response over latitude and altitude. Positive phase shifts represent a delay of the response of water vapour to the solar cycle.

ACPD
15, 12353–12387, 2015

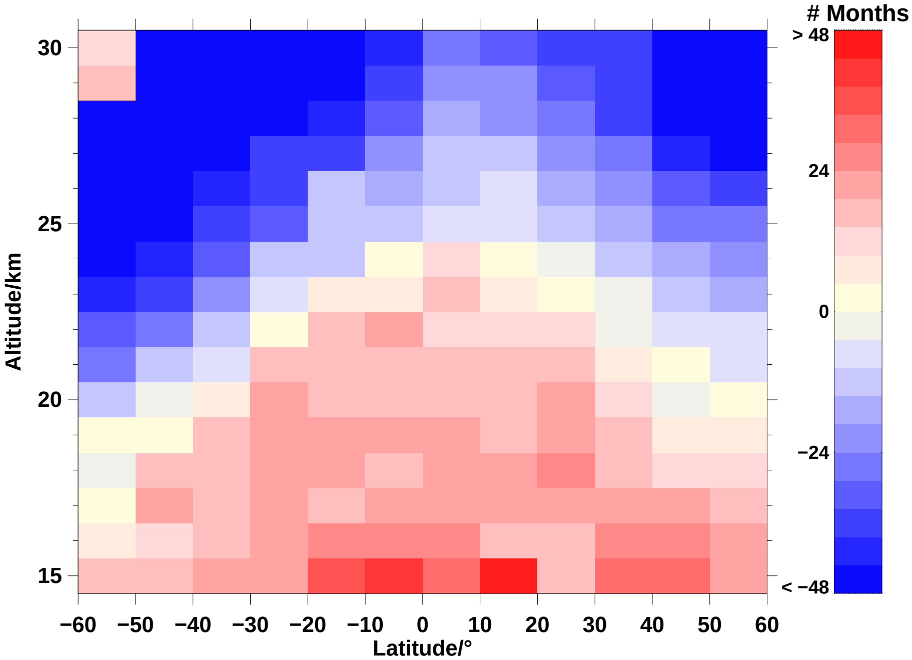

Figure 10. Inherent time lag of the solar signal in water vapour, i.e. difference of the phase shift of the solar signal in water vapour and the age of stratospheric air as derived in Stiller et al. (2012b). Positive values represent delays of the solar signal in water vapour larger than the stratospheric mean age of air.

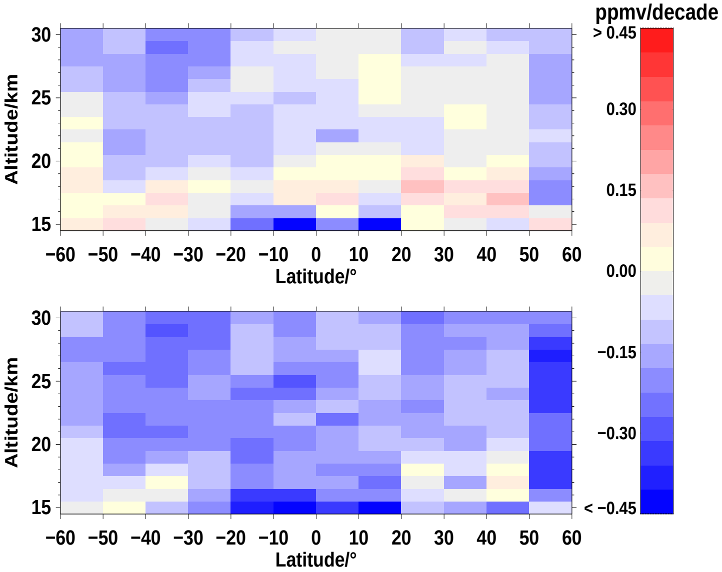

Figure 11. Linear terms of the multivariate regression of water vapour time series with and without the inclusion of a solar term in the regression model. Top panel: standard approach without solar term; lower panel: including F10.7 parametrization.